Developing A CD-CBM Anticipatory Approach For Cavitation – Defining A Model Descriptor Consistent Between Processes

Glenn O. Allgood, Stephen W. Kercel, William B. Dress
Instrumentation and Controls Division
Oak Ridge National Laboratory*
Oak Ridge, TN 37831-6007

ABSTRACT

A major problem with cavitation in pumps and other hydraulic devices is that there is no effective method for detecting or predicting its inception. The traditional approach is to declare the pump in cavitation when the total head pressure drops by some arbitrary value (typically 3%) in response to a reduction in pump inlet pressure. However, the pump is already cavitating at this point. A method is needed in which cavitation events are captured as they occur and characterized by their process dynamics. The object of this research was to identify specific features of cavitation that could be used as a model-based descriptor in a context-dependent condition-based maintenance (CD-CBM) anticipatory prognostic and health assessment model. This descriptor was based on the physics of the phenomena, capturing the salient features of the process dynamics.

An important element of this concept is the development and formulation of the extended process feature vector (*fv*) or model vector. This model-based descriptor encodes the specific information that describes the phenomena and its dynamics and is formulated as a data structure consisting of several elements. The first is a descriptive model abstracting the phenomena. The second is the parameter list associated with the functional model. The third is a figure of merit, a single number between [0,1] representing a confidence factor that the functional model and parameter list actually describes the observed data. Using this as a basis and applying it to the cavitation problem, any given location in a flow loop will have this data structure, differing in value but not content. The extended process feature vector is formulated as follows:

$$fv \Rightarrow [\,\langle f(x,t,)\rangle, \{\text{parameter list}\}, \text{confidence factor}]. \quad (1)$$

For this study, the model that characterized cavitation was a chirped-exponentially decaying sinusoid. Using the parameters defined by this model, the parameter list included frequency, decay, and chirp rate. Based on this, the process feature vector has the form:

$$fv \Rightarrow [\langle e^{-\gamma t}\cos(\omega t+\alpha t^2),\ e^{-\gamma t}\sin(\omega t+\alpha t^2)\rangle,\ \{\omega = a,\ \gamma = b,\ \alpha = c\},\ cf = 0.80]. \quad (2)$$

In this experiment, a reversible catastrophe was examined. The reason for this is that the same catastrophe could be repeated to ensure the statistical significance of the data.

INTRODUCTION

Effective prognostics require a combination of accurate measurements and applicable analytic techniques. Sensor technologies for condition monitoring are fairly mature. The problem, then, resides in the analytic approaches and methodologies applied to collected data. In some instances the data are simply presented

* Managed and operated by Lockheed Martin Energy Research Corporation for the U.S. Department of Energy under Contract DE-AC05-96OR22464.

DISCLAIMER

DISCLAIMER

Portions of this document may be illegible in electronic image products. Images are produced from the best available original document.

to an operator or maintenance expert for subjective interpretation. Often, simple threshold detection is used. If a certain measurement goes out of range, the machine is taken off-line and out of service whether there is a problem or not. This reactive approach is complicated by the fact that machine setup can influence an operator's perception of system health forcing a decision to bring a unit down when no problem exists.

Other conventional signal analysis approaches are based on simple curve fitting and trending of data. This is insufficient for several reasons. First, it discards most of the information generated by the sensor. Second, it makes important control and system operational decisions based on extrapolation. This policy will not meet the optimization demands of today's manufacturers. This is also true of a flow loop since it is well known that catastrophic pump failures occur frequently in practice and are not predicted by extrapolation. This is a generalization supported by other systems. As an example, one manager in the aerospace industry has stated that 85% of aircraft component failures are event driven. The failures occur in context with what the aircraft has been asked to do in order to meet mission needs and has nothing to do with time itself.

Based on these observations, it seems that model-based reasoning has not found its way into the mainstream conventional practice of predictive or condition-based maintenance (CBM). This was highlighted at a National Institute of Standards and Technology workshop on CBM (11/17/98) where it was identified as one of three major research areas for CBM. Others have. Williams, as an example, notes that "The field of neural nets is rapidly growing and is likely to yield useful results in the future but for now there is an element of 'use it and see' about it."[1] Wavelets seem to be gaining in popularity, also.

Standard approaches include Fourier-based spectral analysis.[2] Unfortunately, this technique suffers due to the fact that acoustic signatures of defective pumps are highly nonstationary and Fourier analysis averages these interesting features out. This points to the need for nonlinear models and techniques that can extract and retain signal information and features. One such approach that supports this need is Bayesian estimation.

BAYESIAN PARAMETER ESTIMATION

Bayesian analysis offers an effective method for extracting useful information (extended process feature vector) from experimental data.[3] It drops irrelevant parameters without loss of precision in describing a functional model and fully exploits prior knowledge. Most important, the computation of the most probable values of a parameter set incidentally includes measure of the probability. That is, the calculation produces an estimate of its own goodness. By comparing the goodness of alternative models, the best available description of the underlying reality is obtained. This is the optimal method of obtaining a model from experimental data, or of predicting the occurrence of future events given knowledge from the past, and of improving the prediction of the future as knowledge of the past improves.[4] Bayesian parameter estimation is a straightforward method of induction.

Bayesian parameter estimation describes our best guess of the description of the signal as the weighted sum of several model functions. Its amplitude, or linear parameter, gives the relative contribution of each model function to the overall model. In addition, within each model function, there may be one or more nonlinear parameters. In this technique, the distinguishing feature of a physical effect is the list of model functions and their parameters and represents a more general concept of the "feature vector" of conventional pattern recognition.

There are as many amplitude parameters as model functions but the nonlinear parameters in each model function must be searched for. All the nonlinear parameters are included in the argument of the probability function; the amplitude parameters are implicit in the number of model functions in the model

(the model's dimensions). The time or sampling points are assumed to consist of a sequence of regularly spaced integers from 1 to the length of the data set. If we wish to scale the sampling points, simply include the scale factor as a (known) nonlinear parameter. Thus, the model for a single oscillatory term might be

$$\{1, \cos(\omega t), \sin(\omega t)\} \text{ or } \{1, \cos(2\pi\omega t\kappa), \sin(2\pi\omega t\kappa)\} \tag{3}$$

where κ is a scaling factor that takes the integer samples represented by t to microseconds, for example, letting ω represent the frequency in MHz. In the first expression, ω is the frequency in radians. Consider a model of linear chirp:

$$\{1, \cos(2\pi\omega t\kappa+\alpha\kappa^2t^2), \sin(2\pi\omega t\kappa+\alpha\kappa^2t^2)\}. \tag{4}$$

Here, there are three explicit nonlinear parameters (α, κ, and ω) and three implicit amplitude parameters. One of the nonlinear parameters is known, namely κ, as the time-scale parameter. The two unknown parameters are α and ω, leading to a two-dimensional search or optimization problem in the ω, α-plane. Generally, if there are m unknown nonlinear parameters, the problem becomes a search in an m-dimensional space for the peak of the likelihood function. Should this prove too much of a computational burden, individual nonlinear parameters may be removed by integration in the usual manner. However, this may prove more difficult than a high-dimensional search.

Log likelihood is the log of the Student-t distribution. This assumes integration over all the linear model parameters. The Student-t is computed from the projection of the data onto the orthogonalized model, which should be the same number as the projection of the data onto the model and the inner product of the data vector with itself as

$$S_t = \left[1 - \frac{<d,m>}{<d,d>}\right]^{(M-N)/2}. \tag{5}$$

The projection of the data onto the model is <d,m> and <d,d> is the projection of the data onto itself. The number of functions in the model is represented by M, and N is the number of samples in the vector.

FEATURES OF IMPENDING CAVITATION (THEORY)

If cavitation started when the minimum flow pressure dropped below the vapor pressure of the liquid, then the prediction of the inception of cavitation would be straightforward. However, many physical effects cause the actual inception point to be further from that predicted by this criterion. One of the most troublesome is the effect of surface tension at a nucleation site. Since the liquid can withstand tensions below the vapor pressure, this has to be taken into account. A microbubble of radius, R_N, and surface tension, S, containing only vapor, is in equilibrium if the liquid pressure is $p = p_V - 2S/R_N$. The liquid pressure must fall below this critical point for cavitation to start. Unfortunately, the liquid contains a great many nucleation sites having a great many radii. These vary with the physical situation and the quality of the fluid.[5] Therefore, the onset of cavitation and its precursors must be observed directly.

One approach is to obtain the nuclei number distribution function, $N(R_N)$, such that $N(R_N)dR_N$ is the number of nuclei per unit volume with radii between R_N and $R_N + dR_N$. The problem with this approach is that there is no straightforward way to measure the nuclei distribution.[6] [As an aside, it may be worth considering using acoustic emission (AE)-based technologies to measure this distribution function.]

Air can cause cavitation. Dissolved air will contribute to the partial pressure of the cavitation bubble. As the bubble moves to a region of higher pressure, the vaporized liquid will condense, leaving the air bubble remaining. Air is slow to redissolve.[6] Thus, one of the things that can go wrong with a cavitation experiment in a test loop is that air bubbles from the first pass are not redissolved in the loop. The return leg of the test loop must be long enough and at high enough pressure for the air bubbles to become reabsorbed. Otherwise, the number of nucleation sites will grow rapidly as the experiment runs. It should be noted that cavitation inception data taken without bubble population data are practically useless. Total air content provides a good estimate of bubble population. The bubble population typically increases with total air content.[7] Do we have a practical way of measuring total air content in our experiments? If we want our data to be taken seriously by the mechanical engineering community, we need a practical way of estimating bubble population.

There are several other effects that contribute to resolving the complexity of cavitation.[8] The first is residence time. The cavitation bubble takes a finite time to form. Residence time depends on pump size, flow rate, and temperature. However, if the cavitation nucleus is in the region of low pressure for less than the residence time, the bubble will not form. This has the effect of lowering the critical cavitation number. Turbulence causes localized low pressure significantly below the mean pressure of the flow and is often the site of incipient cavitation. This effect is dependent on the Reynolds number, but is a separate effect from the dependency of the pressure coefficient on the Reynolds number. Turbulence has the effect of raising the critical value of the cavitation number. Surface roughness also creates localized low-pressure perturbations. Localized low pressure is a departure from the simplifying assumption that the pressure is uniform at an average value through a cross section of the stream.

Due to various effects, a pump will have its minimum cavitation inception number at its design flow rate.[9] In the experiment, there is a need to run the flow loop driver pump near its design flow rate to minimize pump cavitation. Even after the pump cavitation bubbles collapse, their residual air bubbles will remain and could lead to excessive nucleation sites in the venturi chamber.

Practically everything that can be said about the properties of the cavitation bubble is based on the Rayleigh-Plesset Equation.[10] To find a solution for the equation is difficult. It may turn out to be more computationally efficient to try to use Bayesian methods to do a direct estimate of the coefficients of this nonlinear differential equation than to try to estimate parameters for its various approximate solutions. The generalized differential equation gives the instantaneous bubble radius, R(t), in response to the driving pressure far from the bubble, $p_\infty(t)$.

$$\underset{(1)}{\frac{p_v(T_\infty)-p_\infty(t)}{\rho_L}}+\underset{(2)}{\frac{p_v(T_B)-p_v(T_\infty)}{\rho_L}}+\underset{(3)}{\frac{p_{Go}}{\rho_L}\left(\frac{T_B}{T_\infty}\right)\left(\frac{R_o}{R}\right)^3} \qquad (6)$$

$$=\underset{(4)}{R\frac{d^2R}{dt^2}}+\underset{(5)}{\frac{3}{2}\left(\frac{dR}{dt}\right)^2}+\underset{(6)}{\frac{4\nu_L}{R}\frac{dR}{dt}}+\underset{(7)}{\frac{2S}{\rho_L R}}$$

The equation is derived based on several simplifying assumptions that turn out to be reasonable in practice. It assumes a single, spherical bubble in an infinite liquid domain whose remote temperature, T_∞, is constant in time. There is no uniform heating of the liquid due to radiation or internal heating. Liquid density, ρ_L, is assumed constant. Dynamic viscosity, μ_L, is assumed constant and uniform. The bubble contents are homogeneous and the temperature, $T_B(t)$, and pressure, $p_B(t)$, inside the bubble are independent of location. It is also assumed the bubble contains a contaminant gas with a partial pressure,

p_{Go}, given a reference bubble radius, R_0, and temperature, T_∞, and that there is negligible mass transfer between the liquid and the contaminant gas.

The driving term depends on the pressure in the liquid far from the bubble, $p_\infty(t)$. The remote vapor pressure of the liquid, $p_vT(_\infty)$, depends only on the liquid and the remote temperature. The liquid density is a property of the liquid. The second term is the thermal term. If thermal effects are to be neglected, then $T_B(t) = T_\infty$, and $p_v(T_B)-p_v(T_\infty) = 0$. When this term is nonzero, it can greatly affect the growth rate of the bubble. The sixth term depends on the kinematic viscosity of the liquid, ν_L. The sixth term depends on the surface tension of the liquid, S.

A consequence of the Rayleigh-Plesset Equation is bubble instability. If the bubble radius is greater than a critical radius, any small perturbation in pressure will cause it to grow without bound. The critical radius is approximately $4S/3(p_v-p_\infty)$. As the pressure, p_∞, drops, the critical radius drops, which means that more nuclei in a given distribution are induced to cavitate. This is why there is a rapid increase in the number of visible bubbles in a cavitating flow as the pressure drops.[11]

In the most simplified case, the solution of the Rayleigh-Plesset Equation will lead to an oscillating response in which the contracting part of the bubble represents a catastrophic collapse. In reality, the oscillation does not occur. As the bubble approaches zero radius, it becomes unstable to nonspherical perturbations; it shatters into a cloud of even smaller bubbles during the first collapse. This generates powerful shock waves that produce AE.[12] The cloud will then expand and collapse and this will also produce powerful shock waves.[13]

The collapse of a bubble near a hard surface produces a microjet directed toward the hard surface and then a collapsing bubble cloud. Due to its high local pressure, the microjet emits noise and causes damage. The collapsing remnant bubble cloud causes even more noise and damage than the microjet, although the mechanism by which it does so is not understood.[14]

The natural frequency at which an isolated bubble oscillates in a quiescent liquid can also be determined from the Rayleigh-Plesset Equation.[15] This suggests the natural frequency should be between 10 kHz and 1 MHz. Acoustic pressure goes as second derivative of bubble volume.

$$\omega_P = \left[\frac{3\bar{p} - p\nu}{\rho_L R_E^2} + \frac{4S}{\rho_L R_E^3} - \frac{8\nu^2}{R_E^4}\right]^{\frac{1}{2}} \tag{7}$$

For an isolated bubble, the second order nonlinear effects have been determined by Kumar and Brennen.[16] The nonlinear differential equation is Equation 8. The solution is Equation 9, as clarified by Equations 10-13. This may be a crude model for a first try at Bayesian estimation. The bubble radius will oscillate at integral harmonics of the excitation, if the excitation is a remote pressure oscillating at a single harmonic frequency. Because the response goes inversely with the order of the harmonic, only the first 50 harmonics contribute to the response. For weak excitation, this model tracks fairly well with a direct numerical solution of Equation 7. More accurate solutions appear in the literature, but this one is easily extended to bubble clouds.

$$R\frac{D^2R}{Dt^2} + \frac{3}{2}\left(\frac{DR}{Dt}\right)^2 + \frac{4\nu}{R}\frac{DR}{Dt} + \frac{2S}{\rho R} = \frac{P_v - P_\chi(t)}{\rho} + \frac{P_{go}}{\rho}\left(\frac{R_o}{R}\right)^{3k} \tag{8}$$

$$\frac{P_n}{\omega_b^2 R_0^2} = \Lambda(n)\frac{R_n}{R_0} + \sum_{j=1}^{n-1}\beta_1(n,J)\frac{R_j}{R_0}\frac{R_{n-j}}{R_0} + \sum_{j=1}^{N-n}\beta_2(n,j)\frac{\overline{R}_j}{R_0}\frac{R_{n+j}}{R_0} \tag{9}$$

$$\omega_b = \left(\frac{3kP_{g0}}{\rho R_0^2} - \frac{2S}{\rho R_0^3}\right)^{\frac{1}{2}} \tag{10}$$

$$\Lambda(n) = \left[\frac{n^2\delta^2}{\omega_b^2} - 1 - i\frac{n\delta}{\omega_b}\frac{4\nu}{\omega_b R_0^2}\right] \tag{11}$$

$$\beta_1(n,j) = \frac{3k+1}{4} + \frac{3k-1}{2}\frac{S}{\rho\omega_b^2 R_0^3} + \frac{1}{2}\frac{\delta^2}{\omega_b^2}(n-j)\left(n+\frac{j}{2}\right) + i\frac{2\nu}{\omega_b R_0^2}\frac{\delta}{\omega_b}(n-j) \tag{12}$$

$$\beta_2(n,j) = \frac{3k+1}{2} + (3k-1)\frac{S}{\rho\omega_b^2 R_0^3} + \frac{1}{2}\frac{\delta^2}{\omega_b^2}\left(n^2 - nj - j^2\right) + i\frac{2\nu}{\omega_b R_0^2}\frac{n\delta}{\omega_b} \tag{13}$$

The acoustic signature of cavitation noise is broadband and has been subjected to various theoretical and experimental investigations. It is noteworthy that practically all experimental results are reported as a power spectral density derived from a Fourier analysis of the data.[17] There appears to be no report in the literature of the fine details in frequency resolution that could be obtained from Bayesian analysis or the transient details that would emerge from wavelet analysis.

The conventional understanding of the character of the acoustic signature is as follows. The dominant frequency is related to the natural frequency of the typical cavitation bubble. This is in turn related to the size of the nucleation site, but there are many nucleation sites and they have a distribution of sizes. There is a critical frequency, f, such that $ft_{TC} = 1$, where $t_{TC} = 0.915R_0[\rho_L/(p_\infty - p_V)]$, is the collapse time of the bubble whose most probable nucleation radius is R_0. At the critical frequency, the power spectral density is highest. Well below the critical frequency, the power spectral density increases as f^4. Well above the critical frequency, the power spectral density decreases approximately as $1/f^2$. Different researchers have reported different results for the complex behavior near the critical frequency. [It would be of great interest to examine this region using Bayesian analysis.]

As cavitation becomes severe, the cavitation bubbles cannot be assumed to act independently of each other.[16] A cloud of interacting bubbles forms. This is a serious concern because the collapse of the bubble cloud causes considerably more damage than the collapse of an isolated bubble. The natural frequency of the bubble cloud is a fraction of the individual bubble.[18] Hence, it is expected that the frequency of AE should drop as cavitation becomes more severe. There is anecdotal evidence this kind of behavior does occur.

It is noteworthy that in a bubbly liquid medium for natural frequencies above 200 kHz, the attenuation of the pressure wave is about 5 dB/cm, as compared to 25 dB/cm at the average bubble natural frequency of 100 kHz. Thus, even if the higher frequency effects may occur less commonly, they may still be as easy to observe as the low frequency events that start out stronger. Another way to interpret this is to note that although most of the energy is generated near the average bubble natural frequency, these bubbles act as absorbers. Energy from the collapse of bubbles far away from the average size is smaller. But since it is not so strongly absorbed, it may be easier to detect.[19]

In a bubbly flow, there is a shock wave. Viscosity will affect the properties of the shock wave and lead to damping effects. For reasonably low void fractions, the shock wave ringing effect occurs at about half the natural frequency of the isolated bubble. In the time domain, at a stationary observation point, the shock wave will be perceived as a rising and then damped nonlinear oscillation. The shock wave contributes to the acoustic signature in cavitating flows. Equation 14 may be particularly relevant to the Bayesian analysis suggested for Phase II.[20]

$$\left(1-\alpha_1+\alpha_1 r^3\right)^2 r\frac{d^2r}{dz^2}+\frac{3}{2}\left(1-\alpha_1+\alpha_1 r^3\right)\left(1-\alpha_1+3\alpha_1 r^3\right)\left(\frac{dr}{dz}\right)^2$$
$$+\left(1-\alpha_1+\alpha_1 r^3\right)\frac{4\nu_L}{u_1 R_1}\frac{1}{r}\frac{dr}{dz}+\alpha_1\left(1-\alpha_1\right)\left(1-r^3\right)$$
$$=\frac{1}{u_1^2}\left[\frac{p_1-pv}{\rho_L}\left(r^{-3k}-1\right)\frac{2S}{\rho_L R_1}\left(r^{-3k}-r^{-1}\right)\right] \qquad (14)$$

The situation that is likely to be encountered is the oscillating, flowing bubble cloud. This will have a number of modes and a number of natural frequencies, all lower than the natural frequency of an isolated bubble. For a small void fraction, all the cloud natural frequencies will be in a narrow range just below the isolated bubble natural frequency. For a large void fraction, the cloud natural frequencies will occupy a large range below the bubble natural frequency. Since damping is strong near the isolated bubble natural frequency and since the outside of the cloud shields the rest of the world from effects inside the cloud, the dominant effect in a cloud in a damping medium is the response at the lowest cloud natural frequency. Thus, the response will be seen as a large peak at the lowest cloud natural frequency and a smaller peak at the bubble natural frequency, with the strength and frequency of the cloud response decreasing with increasing void fraction.[21]

Notice the foregoing paragraph only describes the linear effects of a bubble cloud in a flow. Other effects at higher frequencies occur when nonlinear effects are taken into account. Harmonic cascading is the effect of harmonics at relatively low frequencies exciting the natural frequencies of smaller bubbles, leading to higher frequency effects. Whereas the linearized analysis of bubble cloud dynamics showed the lowest cloud natural frequency as the dominant effect. Nonlinear analysis says the low-order harmonics of the lowest cloud natural frequency are also strongly present. This can stimulate harmonic cascading if the fluid contains nucleation sites over a range of small sizes. Fine resolution at high frequencies is needed to observe harmonic cascading. Previous researchers typically used Fourier analysis at 1/3-octave resolution to analyze experimental data.[16] Bayesian methods should dramatically reveal harmonic cascading. In addition, if the bubbles are not spherical, super-resonant effects can occur.[22]

Note that the isolated bubble natural frequency is the key to understanding the expected acoustic effects of a cavitating flow. The distribution of sizes of nucleation sites will cause AE to be spread out about the

natural frequency of the average nucleation radius. The shock wave will produce a strong signature in the region 0.1-0.9 of the isolated bubble natural frequency. The cloud effects will produce more energy just below the natural frequency.[16]

If the strength of excitation is such that the weakly nonlinear solution applies, then the response will be one of the following conditions. The response is *subresonant* if the excitation is at a frequency lower than the lowest natural frequency of the bubble cloud. The response is *transresonant* if the excitation is at a frequency higher than the lowest natural frequency of the bubble cloud, but lower than the natural frequency of the average bubble in the cloud. The response is *super-resonant* if the excitation is at a frequency higher than the natural frequency of the average bubble in the cloud. Super-resonance response decays fairly rapidly with distance from the source of excitation. It is strongest in the center of the cloud and weakens toward the edges.[16]

The harmonic cascade is predicted by Kumar.[16] Harmonic cascades should be a common occurrence in practical experiments. High-resolution frequency spectra should reveal them.[23]

EXPERIMENTAL RESULTS

The observables measured in this experiment are the broadband AE signatures of a venturi chamber in a flow loop. The AE data are known to contain features of incipient cavitation and are suspected of containing features of impending cavitation.[23] Previous experimenters have reported unmistakable features of incipient cavitation, but concluded that much richer information was being lost due to the limitations of the then-available hardware.

To search for features of impending and incipient cavitation in AE data, the experiment reported in this paper began where the work of Neill et al. left off. The authors used a flow loop at Oak Ridge National Laboratory that is routinely used for calibrating various flow devices. The source of AE signatures was a venturi chamber inserted into the flow loop. The venturi chamber was designed specifically for this experiment and is similar to the one described by Neill et al.

The authors used a Vallen Systeme AMSY4-MC6 AE monitor (Vallen ID number 40900) to collect the data. A complete set of AE signatures at various flow rates was collected with broadband piezo-electric AE sensors (Vallen SE-1025-H, usable frequency response from 10 kHz through greater than 400 kHz). Another complete set of AE signatures at various flow rates was collected with narrowband piezo-electric AE sensors (Vallen SE-9125-M, usable frequency response from 20 kHz through 200 kHz). Sampling rate was 10 million samples per second. Dynamic range was approximately 80 dB. This paper includes highlights from the experimental data.

A typical example of the time-domain signature of a cavitation event seen in the AE data is shown in Figure 1. This type of signature occurs very frequently at high flow rates (thousands of instances per second at flow rates above 20 gallons per minute (gpm)). This is a particularly clean instance from the unrefined raw data of the many cavitation events observed at 30 gpm and is used to derive a model of the cavitation event. The amplitude is normalized to 1 at the peak value of the signature. The time-axis is in units of μ sec.

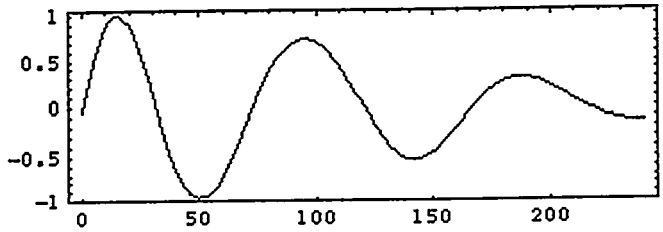

Figure 1. AE signature at 30 gpm.

A linear-chirped damped sinusoid is easily fitted to these data. The model is $\{e^{-\gamma t}\cos(\omega t\kappa+\alpha\kappa^2t^2),\ e^{-\gamma t}\sin(\omega t\kappa+\alpha\kappa^2t^2)\}$. Assume $\kappa=1$. Bayesian parameter estimation computes the most probable nonlinear parameter values are $\omega = 0.0877091$, $\alpha = -0.000923205$, and $\gamma = 0.00553404$. As shown in Figure 2, this provides a very good first order fit to the data. The damped chirp model is used in the subsequent analyses in this paper. The utility of a more sophisticated model (nonlinear chirps and other decay envelopes) to describe these data will be investigated in future research.

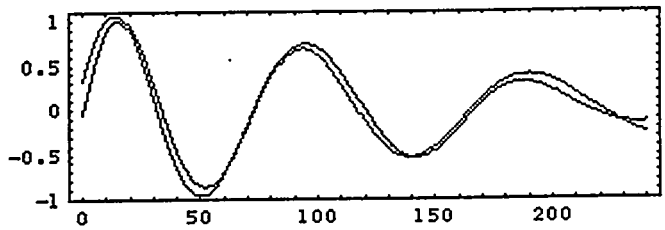

Figure 2. Fitted damped chirp model and observed data.

Figure 3 shows a typical frame of data captured at 30 gpm with the narrowband sensor. From the audible crackling from the venturi chamber, we know that severe cavitation was occurring. Figure 3 shows a little over 2000 μ sec of data with maximum amplitude of approximately 20,000 μV. [Note: In Figures 3, 5, 7, and 9, the vertical-axis is the raw AE sensor output in μV.]

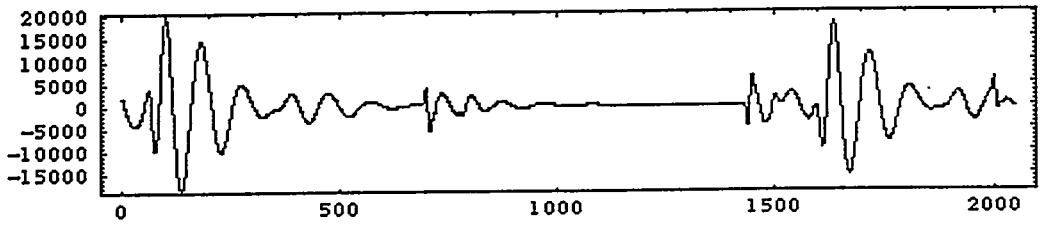

Figure 3. Several cavitation events at 30 gpm.

Likelihood is computed for each set of 240 data points in the signature data as the model (used as a matched filter) is swept forward one sample at a time. The nonlinear parameters and then the linear parameters are calculated for the model and the goodness of the fit is determined by computing the log (likelihood) in dB. As shown in Figure 4, the signature of Figure 3 includes four events that are very likely damped chirp events. Similar data are shown in Figures 5 and 6 at a 20 gpm flow rate.

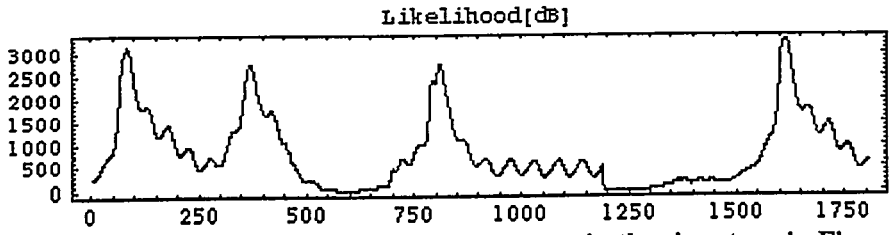

Figure 4. Likelihood of damped chirp events in the signature in Figure 3.

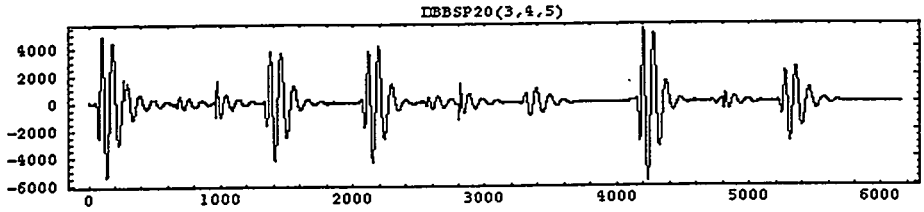

Figure 5. Several cavitation events at 20 gpm.

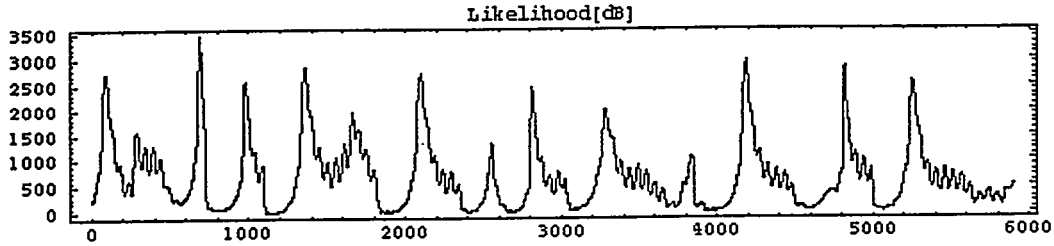

Figure 6. Likelihood of damped chirp events in the signature in Figure 5.

At flow rates below 18 gpm, damped chirp features are very rare occurrences. As Figures 7 and 8 show, a typical data set collected at 17 gpm is practically indistinguishable from the electronic noise of the experimental setup. [Note: The noise floor of the electronics is 1 μV root mean square.]

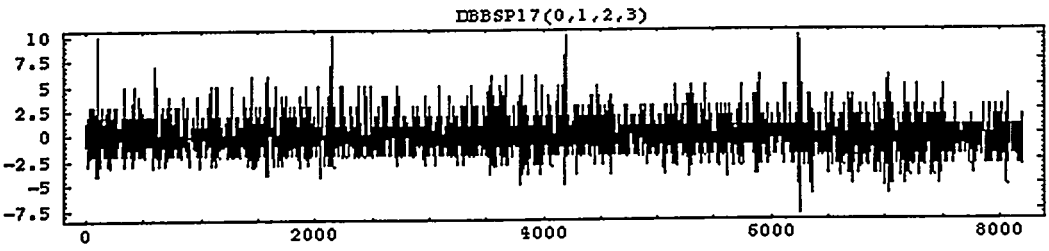

Figure 7. Typical data set at 17 gpm.

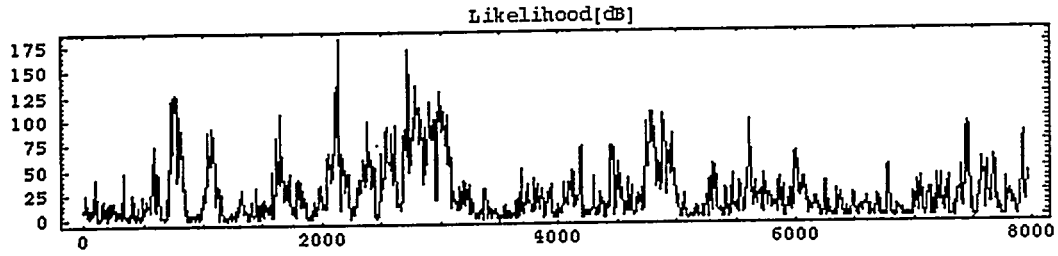

Figure 8. Likelihood of damped chirp events in the signature in Figure 7.

Compare Figures 7 and 8 with Figures 9 and 10. Figure 9 is a typical time domain signature with the sensors mounted on the venturi section, but with zero flow through the flow loop. This is the AE signature of the noise from the environment plus the experimental apparatus itself. As seen in Figure 10, if the log likelihood measure is below 750, it is very unlikely that a damped chirp feature is present in the data.

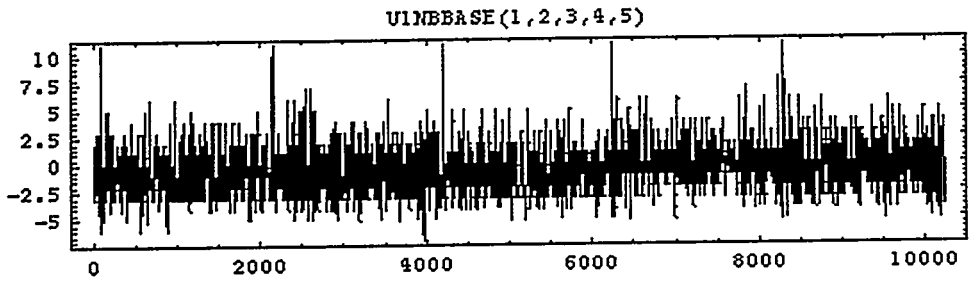

Figure 9. Typical data set at zero flow.

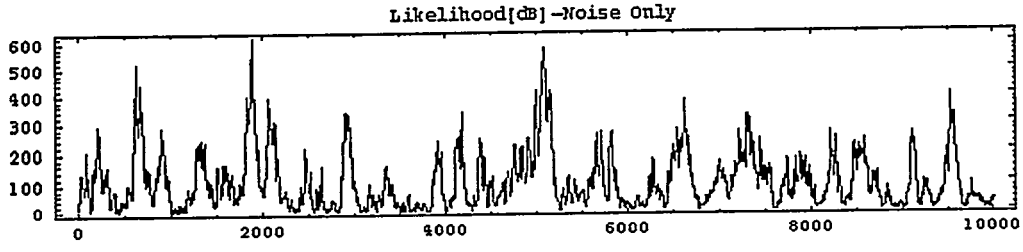

Figure 10. Likelihood of damped chirp events in the signature in Figure 9.

Although damped chirps are rare at 17 gpm, they do occur occasionally. Figure 11 (time domain shown higher, likelihood shown lower) shows the only event captured at 17 gpm with the broadband sensors that do not look just like noise. Bursts are apparent in the time domain data; a stronger burst near the beginning and a weaker one just after the strong one. Both are only a little stronger than the background noise.

Figure 12 shows more details of the log likelihood plot from Figure 11. It is noteworthy that the weaker burst between times 700 and 900 is more likely to be a damped chirp than the stronger burst between times 200 and 400. If the "threshold of cavitation" is between 17 and 18 gpm, it is possible the very weak damped chirp (amplitude on the order of 10 μV) in the 17 gpm data is a precursor to the very strong

damped chirp (amplitude on the order of 10 mV) signature in the data at 18 gpm and above. This needs to be investigated in more detail in subsequent research.

Comparing the 17 gpm data with the zero flow data, it appears that a crude way to distinguish between the presence and absence of damped chirps is to use the log likelihood of 750 as a threshold. The damped chirp appears to be a cavitation signature, although this remains to be confirmed by further investigation. Weak damped chirps (amplitudes of approximately 10 μV with this experimental setup) with a high log likelihood (greater than 750) appear to be a useful cavitation precursor.

In future work, a less crude (and more reliable) method of deciding whether or not the cavitation signature is present would be a Rosen anticipation engine. The interacting models in the Rosen anticipation engine would be derived from experimental data similar to these and the theory already described. Such a system would inductively learn the signature of cavitation, with the effectiveness of the learning improving over time as the anticipation engine gains experience.

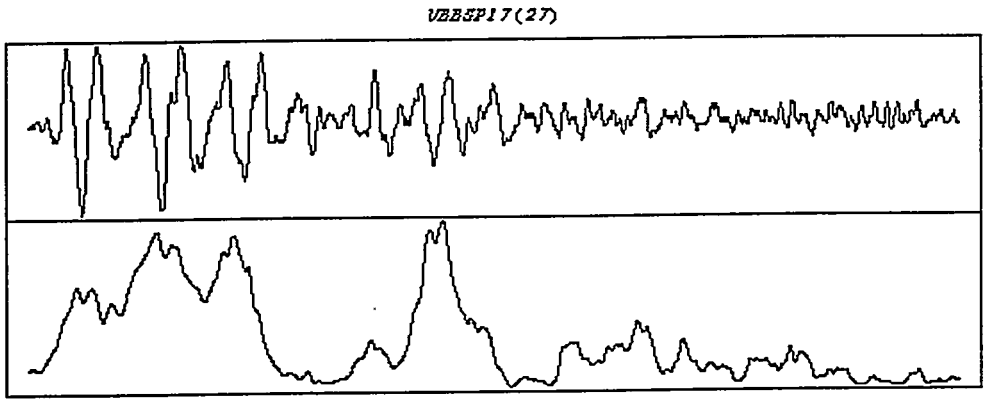

Figure 11. A possible damped chirp at 17 gpm.

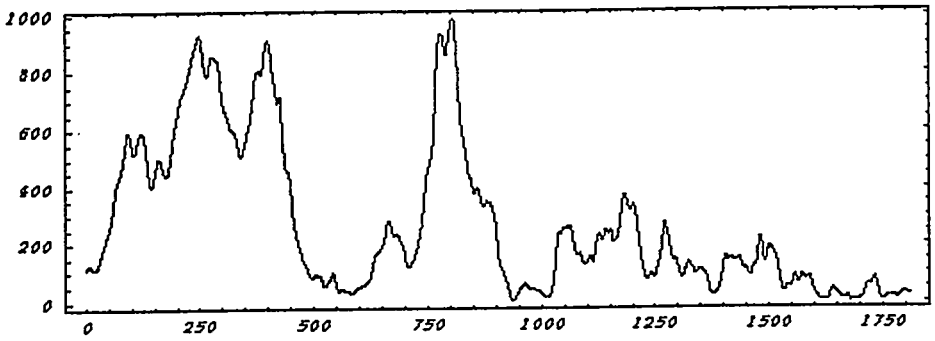

Figure 12. Log likelihood of damped chirp at 17 gpm.

A bit of interpretation of the data yields some useful guidance at this point. The dominant frequencies of the damped chirps are in the digital frequency range of $0.08 <= \omega <= 0.1$ radians. The sampling rate is 10^7 samples per second, meaning the digital frequency of π corresponds to 5 MHz. Thus, the underlying dominant frequency of the physical chirps is in the range of 127-159 kHz. This is well within the flat response range of the broadband AE sensors. It is also in the resonance peak of the narrowband sensors whose sensitivity in the resonant band tends to be 5-15 dB greater than the sensitivity of the broadband

sensors. This suggests that at flow rates below 17 gpm, we should see occasional weak high-likelihood damped chirps with the narrowband sensors. We did.

For example, consider the data set shown in Figure 13, observed at 14 gpm with the narrowband sensors. Note that the two bursts most likely to be damped chirps are barely stronger than the noise and the matched filter does not show a strong response to the much stronger signal that is unlikely to be a damped chirp.

Figure 14 shows more details of the log likelihood plot. It is noteworthy that three very weak damped chirps (amplitude below 10 μV) in the 14 gpm data are very likely to be damped chirps. It is also noteworthy that the strong burst at the beginning of the time domain signal is unlikely to be a damped chirp. Among other things, this illustrates that Bayesian parameter estimation does not confuse strong undesired signals with the damped chirp. Similar results are seen at 13 gpm, but the events are rarer and weaker than at higher flow rates.

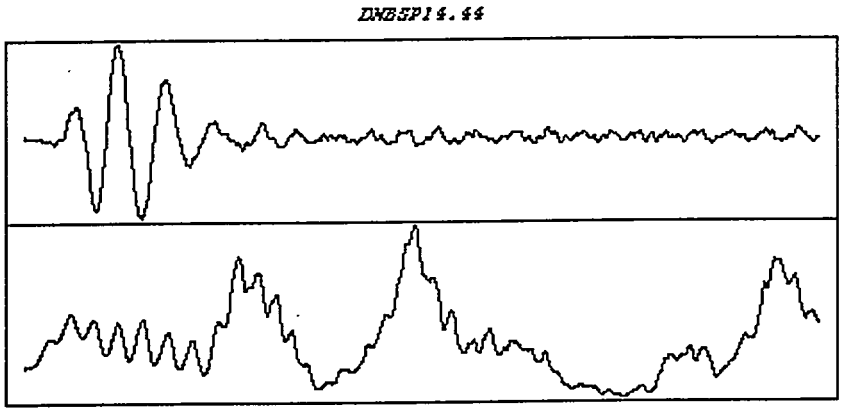

Figure 13. Likely damped chirps at 14 gpm in narrowband data.

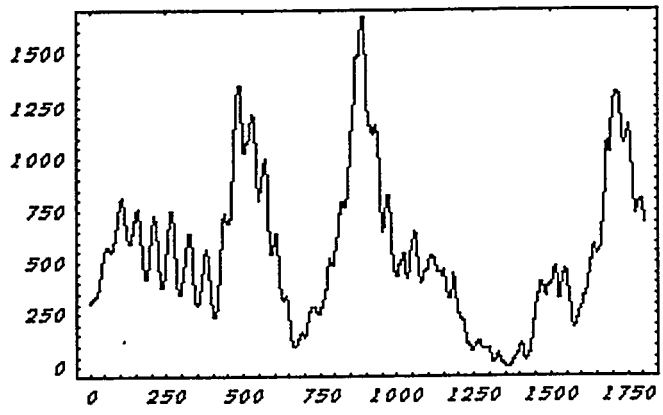

Figure 14. Log likelihood of damped chirps at 14 gpm.

CONCLUSIONS AND FURTHER RESEARCH

The conclusions drawn from this study are listed below.

1. Damped chirped AE signatures are a distinguishing feature for cavitation occurring above and below the inception threshold.
2. Damped chirped signals are easy to detect and hard to confuse with other events using Bayesian parameter estimation.
3. These features (or descriptors) can be used as event precursors to eliminate inception of cavitation, considered a catastrophic event.
4. At flow rates below the threshold of cavitation, occasional damped chirps are observed with weak amplitudes (virtually indistinguishable from noise), but high log-likelihood measures.

These conclusions have utility in two aspects of cavitation detection. First, it appears the sudden appearance of strong damped chirps in response to a small increase in flow rate is a strong and reliable indicator of the inception of cavitation. Second, weak damped chirps at low flow rates appear to be cavitation precursors. This suggests the Bayesian-derived damped chirp may be well suited to be a model in the anticipation engine.

ACKNOWLEDGMENTS

This research was a joint research effort with AEPTEC Microsystems, Inc., supported under their SBIR No. N98-114.

REFERENCES

[1] John H. Williams, Alan Davies, and Paul R. Drake, *Condition-based Maintenance and Machine Diagnostics*, Chapman and Hall, London, 1994.
[2] R. H. Green and D. A. Casada, *Detection of Pump Degradation*, NUREG/CR-6089, 1995.
[3] L. Bretthorst, *Bayesian Spectrum Analysis and Parameter Estimation*, pp. 1-5, Springer-Verlag, Berlin, 1988.
[4] E. T. Jaynes, "Generalized Scattering," in *Maximum-Entropy and Bayesian Methods in Inverse Problems*, C. R Smith and W. T. Grandy, Editors, pp. 377-398, D. Reidel Publishing Co., Holland, 1985.
[5] Christopher E. Brennen, *Hydrodynamics of Pumps*, pp. 74-76, Oxford University Press, Oxford, 1994.
[6] Ibid., p. 76.
[7] Ibid., pp. 89-90.
[8] Ibid., p. 78.
[9] Ibid., pp. 92-93.
[10] Christopher E. Brennen, *Cavitation and Bubble Dynamics*, pp. 34-37, Equation 2.12, Oxford University Press, Oxford, 1995.
[11] Ibid., pp. 43-48.
[12] Brennen, *Hydrodynamics*, pp. 99-104.
[13] Brennen, *Cavitation*, pp. 79-80.
[14] Brennen, *Hydrodynamics*, pp. 108-111.
[15] Brennen, *Hydrodynamics*, pp. 111-118, Equations 6.14 and 6.15.
[16] S. Kumar and C. E. Brennen, "Some Non-Linear Interactive Effects in Bubbly Cavitation Clouds," *Journal of Fluid Mechanics*, Vol. 253, pp. 565-591, 1993.
[17] Brennen, *Cavitation*, pp. 83-91.
[18] Ibid., pp. 193-201.
[19] Brennen, *Cavitation*, pp. 182-187.
[20] Ibid., pp. 188-193, Equation 6.72.
[21] Brennen, *Cavitation*, pp. 194-201.
[22] L. d'Agostino, C. E. Brennen, and A. J. Acosta, "Linearized Dynamics of Two-dimensional Bubbly and Cavitating Flows Over Slender Surfaces," *Journal of Fluid Mechanics*, Vol. 192, pp. 485-509, 1988.

[23] G. D. Neill, R. L. Reuben, P. M. Sanford, E. R. Brown, and J. A. Steel, "Detection of incipient cavitation in pumps using acoustic emission," *Proceedings of the Institution of Mechanical Engineers*, Part E, Vol. 211, pp. 267-277, 1997.